



Experimental analysis of single layer multi-track deposition of clad beads with variable overlap percentages

Parvaneh Zareh¹ · R. J. Urbanic¹

Received: 11 April 2020 / Accepted: 19 June 2020 / Published online: 17 July 2020
© Springer-Verlag London Ltd., part of Springer Nature 2020

Abstract

Controlling the quality of a laser clad bead is one of the most important goals for the cladding process. The quality of the bead is predominantly affected by the process parameters, but the travel path operating parameters also influences the resultant geometry and mechanical properties. An experimental approach to investigate the mechanical properties of beads with variable overlap conditions is presented in this paper. This scenario occurs frequently but has not been investigated. Using the direct energy deposition (or laser cladding) process, 420 stainless steel beads are deposited onto mild steel. One-bead, two-bead, and four-bead configurations are evaluated for two different sample lengths. The percent overlap varied between 30 and 47% for the multi-bead samples. The bead geometry, hardness, and distortion results are collected and analysed. The percentage overlap impacts the hardness and the melt pool depth. The number of beads influences both those characteristics as well as the distortion. The sample length influences the distortion. These experiment data sets serve as the foundation for a calibrated finite element model.

Keywords Additive manufacturing · Metal · Direct energy deposition (laser cladding) · Experimental · Variable overlap · 420 stainless steel, hardness, distortion

1 Introduction

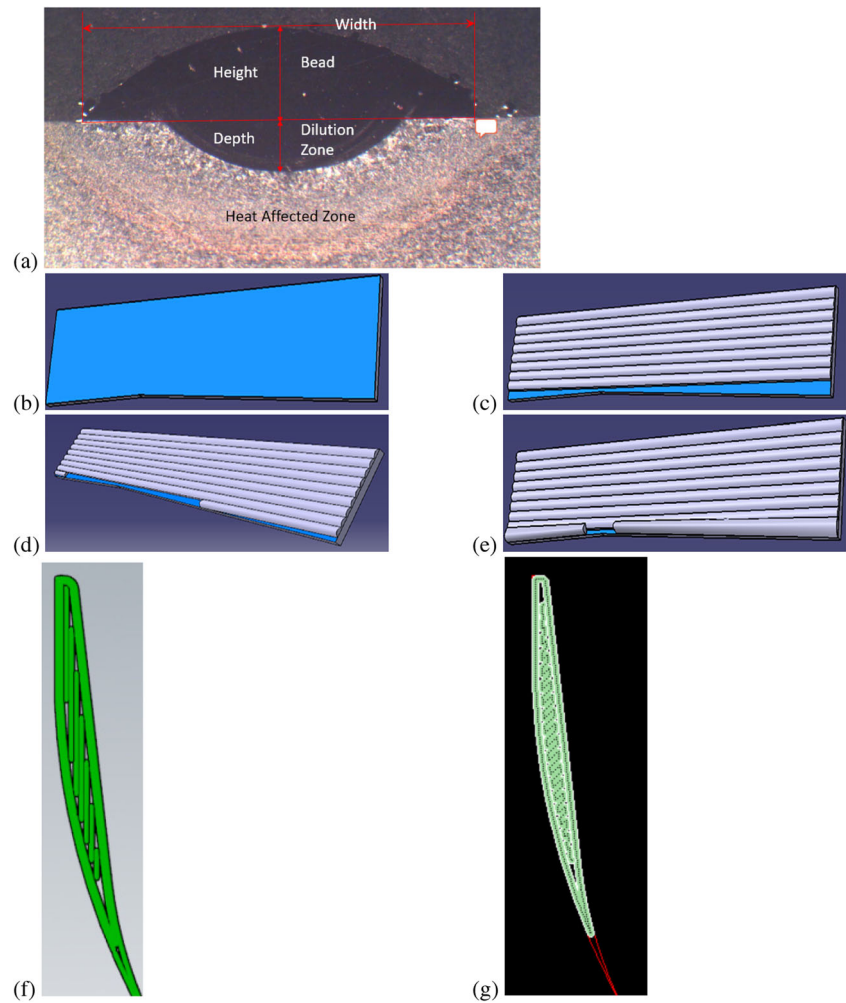
Laser cladding is defined as the process of depositing one material onto the surface of another using a laser as the heat source for melting the deposited material. This process has highly controlled energy input characteristics. It is one of the advanced technologies used to apply the protective coatings. This process can be used to deposit clad layers to achieve high hardness, good wear resistance, and high resistance to oxidation [1]. Laser cladding also can be utilized to generate near-net shapes to build high-precision repair coatings for critical high-value parts [2, 3]. Fundamental research related to linking the process parameters to bead geometry has been performed by several researchers to develop a foundation for the process planning

[4–6] and is still not a mature area of research. Recently, Nabhani et al. [7] investigated cladding parameter effects on the appearance of cladding beads and developed the empirical-statistical model to predict the geometrical characteristics. Complementary research assessing geometry along with microstructure is presented by Tran et al. [8]. They built a three-dimensional thermal model of laser cladding process to anticipate the depth of the melt pool and investigated the phases' formation mechanisms in the layers through evaluating the temperature distributions. Several researchers have explored component fabrication using amorphous, brittle, and hard to manufacture materials to generate a high quality clad surface or an expected near-net shape. Wang et al. explored the microstructure and wear resistance for cladding Ti for repair applications [9]. Some researchers [10, 11] produced composite coatings to improve the hardness of cladding layers for Ti alloys in addition to the evaluating process parameters (laser power and scanning velocity). In addition to considering alloying elements and process parameters, it has been determined that the microstructure and hardness of the cladding layers were affected by cladding tool paths [12, 13]. Homogeneous microstructures can be reached by having a

✉ R. J. Urbanic
jurbanic@uwindsor.ca
Parvaneh Zareh
zareh@uwindsor.ca

¹ Department of Mechanical, Automotive, and Materials Engineering, University of Windsor, Windsor, Ontario N9B 3P4, Canada

Fig. 1 **a** Bead nomenclature, **b** shape to be coated, **c** constant overlap solution (note void could be pushed into the interior), **d** and **e** partial overlap solutions, **f** thin-walled complex shape voids caused by the tool path deposition pattern with default settings using APlus® before the void fill algorithm, and **g** using the Stratsys Insight® software



constant tool path length [13]. Farayibi et al. [14] optimized process parameters to decrease inter-run pores in overlapping clad beads. Nazemi et al. [15] considered hardness in multi-track laser cladding models with 40%, 50%, and 60% overlap and found out that in all cases, the hardness decreased from the first bead to the third bead. The highest average of hardness for the first, second, and third bead belonged to the 60%, 40%, and 50% overlap, respectively. However, they determined that the hardness varies at the joint between beads and the inter-joint hardness also was influenced by the percentage overlap [12].

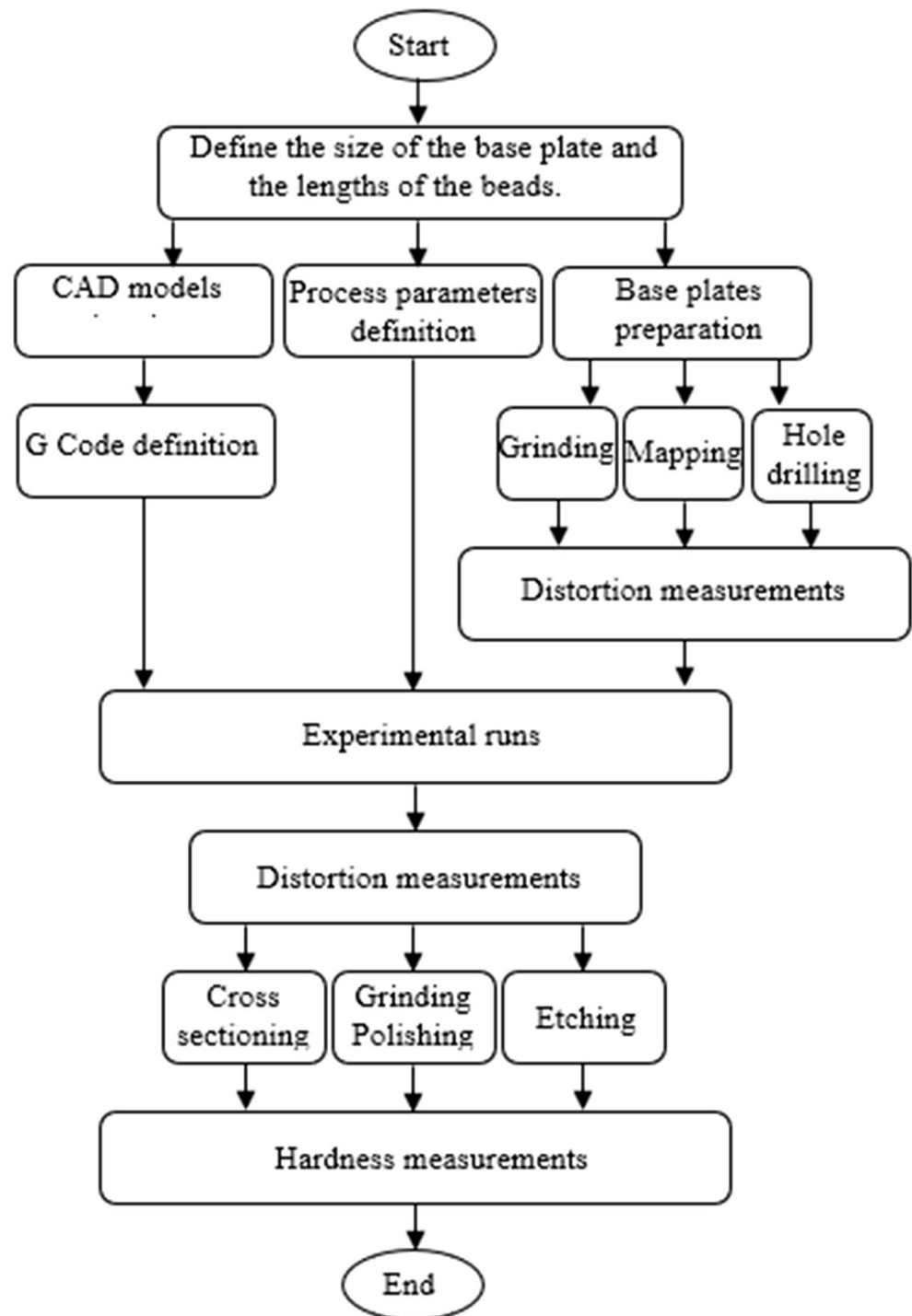
In addition to the hardness characteristics, the distortion is also a resultant of the heat input and influences the global

shape behaviours. Lindgren et al. [16] investigated welding distortion and residual stress formation by utilizing finite element methods. Chiumenti et al. [17] considered the ways that laser cladding process can influence final distortion quantities to find the final mechanical properties that resulted from different deposition passes. Fessler et al. [18] investigated the sequences of the deposition passes. Klingbeil et al. [19] considered the effects of pre-heating on the final distortion. Vayre et al. [20] analysed the fixturing effects on distortion. All the researchers used a variety of different materials and different process parameters. Although they checked the final distortion, they did not consider the accumulation of distortion during the cladding process. Grum et al. [21] measured the strain

Table 1 Chemical composition of the substrate and cladding powder

Elements	C%	Si%	Mn%	P%	S%	Cr%	Ni%	Cu%	Sn%	Co%
AISI 1018	0.18	0.19	0.81	0.012	0.033	0.1	0.14	0.23	0.01	-
AISI 420	0.23	0.5	1.5	0.04	0.03	12.6	-	-	-	0.02

Fig. 2 Experimental process flow



evolution during the laser cladding process for different deposition patterns and laser energy. Plati et al. [22] used their model to measure deformation and found that plastic deformation causes residual stresses generation also led to residual distortion of the workpiece. Ocelík et al. [23] measured in situ strain and deformation during single and multi-pass laser cladding with several powder materials and used steel and stainless steel as substrate. They determined that the displacement

at the beginning and the end of the laser tracks were approximately the same, which showed the plate bending symmetry. A study performed by Nazemi and Urbanic [12] explored the influence of the tool path on distortion and clearly indicated that the deposition patterns (spiral compared to raster fill) impact the resultant distortion.

To date, no study on the impact of variable overlapping has been reported. Some researchers [24–26] have investigated

Table 2 Experimental process parameters

Process parameters	Units or notes
Heat source power	2400 W
Heat source type	Gaussian distribution
Scanning speed	15 mm/s
Scanning pattern	One way
Contact tip to workpiece distance	23 mm
Laser return time	2 s
Start overlap percentage	30%
End overlap percentage	47%
Focal length of lens	400 mm
Ambient temperature	20 °C
Number of replicates	3

multi-track bead configurations with constant overlap beads both experimentally and by simulation and have considered the effects of different input parameters on the mechanical and metallurgical properties of the components. However, most of

the parts which are being coated or built up by laser cladding do not have rectangular surfaces. Their complex geometry makes the generation of coating tool paths complicated. Multi-track beads with a constant overlap percentage cannot be a solution. In this study a solution to reduce the uncoated spots on the substrate surface is introduced. Figure 1 a shows the shape of a standard bead and the nomenclature. Figure 1 b illustrates a substrate which needs to be coated with a variable overlap percentage in some regions. By depositing beads with a constant overlap percentage (Fig. 1c), there are still uncovered regions. However, variable overlapping as shown in Fig. 1 d and e reduces these regions. Void or underfill regions can be in the interior, as shown in Fig. 1 f and g. Coating complex parts is a common problem in industry. The problem is greater for products to be made by an additive manufacturing approach and for surface cladding scenarios. However, a variable solution to eliminate this problem has not been investigated previously.

The long-term goal of this research is to model 3D parts generated by stacking clad bead layers and predicting the re-

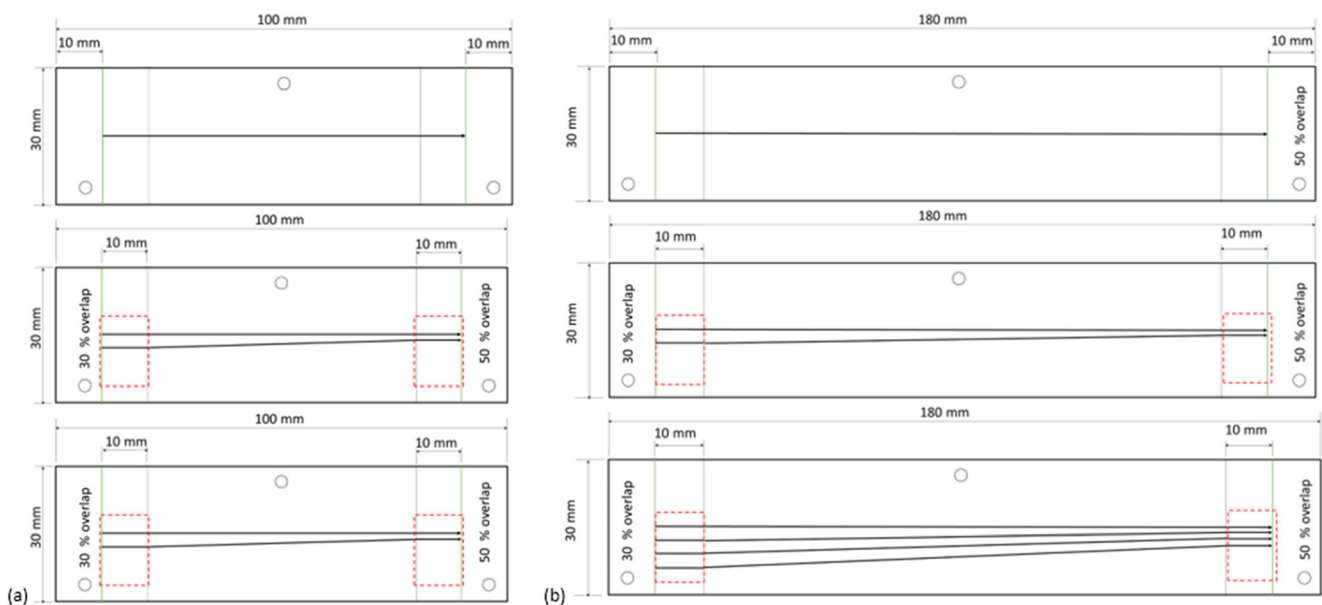
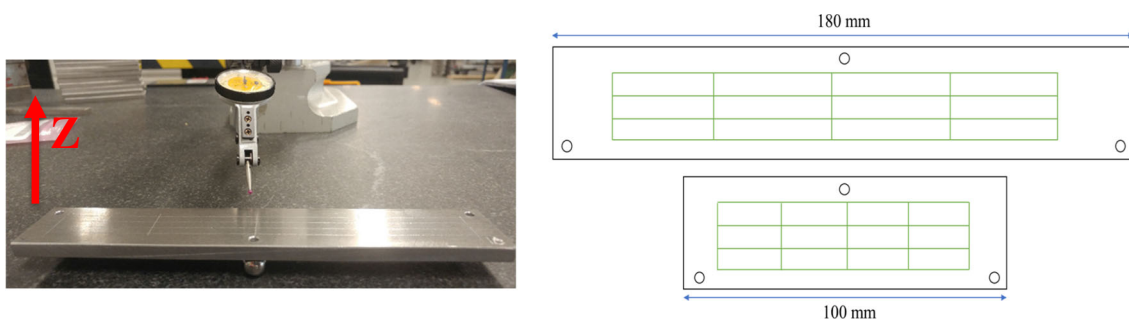
**Fig. 3** Diagram of the cladding strategy with the tool path directions**Fig. 4** a Height gage used for distortion measurements, b the direction of distortion measurement

Fig. 5 Displacement of the plates before the experiments with **a** 100-mm length and **b** 180-mm length

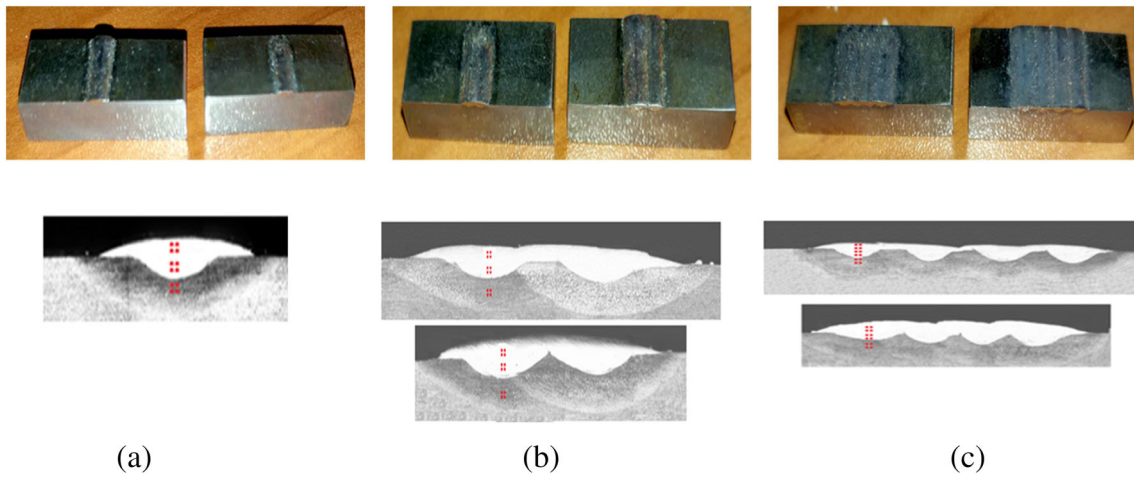
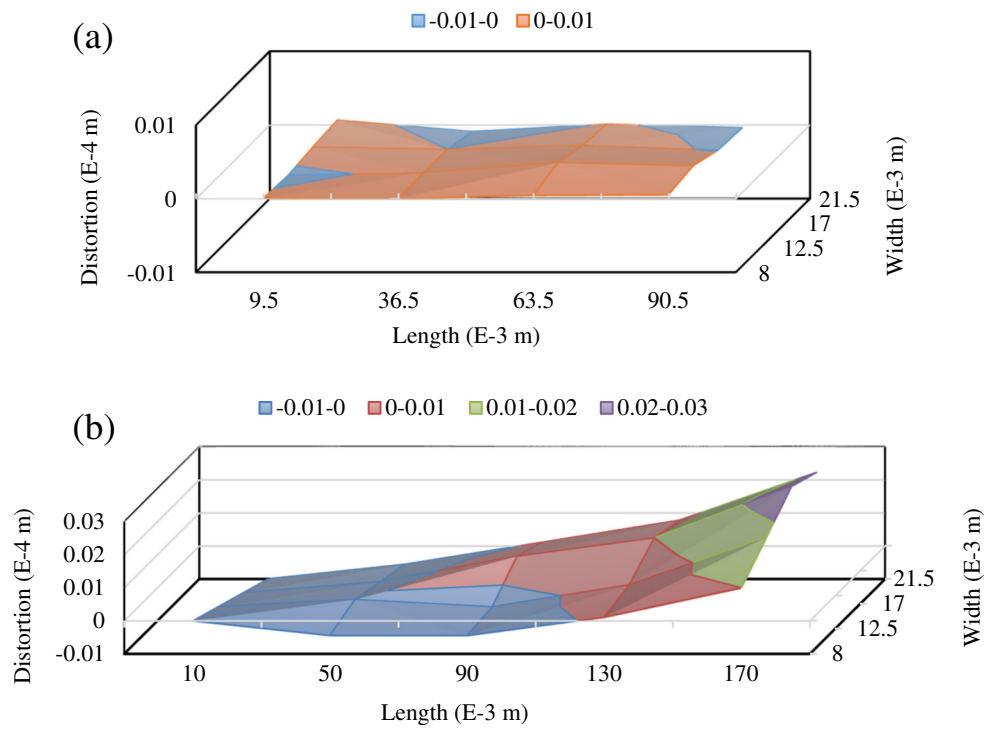


Fig. 6 **a** Cross-sections of single-bead models. **b** Cross-sections of multi-track models with two beads. **c** Cross-sections of multi-track models with four beads

Fig. 7 Sample overlapping bead experiments: **a** 2 beads, 180-mm plate; **b** 2 beads, 180-mm plate; **c** 2 beads, 100-mm plate; **d** 4 beads, 100-mm plate

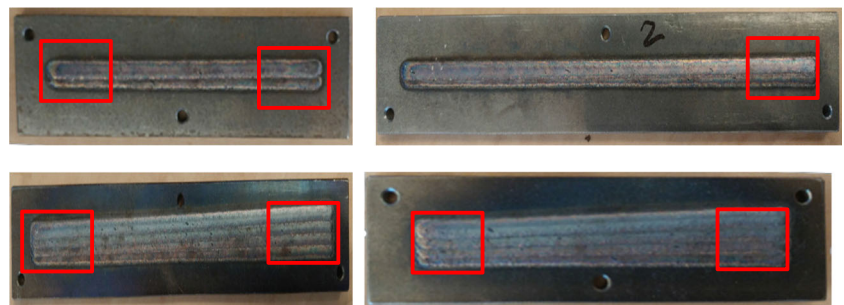


Table 3 The absolute geometry data

Geometry measurements						
Row	no.		Averaged bead heights (mm)	Width of beads in each cross-section (mm)	Approximated width (mm)	
		Width standard deviation				
1	Single track		0.41	4.12	7.80E-03	
2	Two beads	30% overlap cross-section	0.41	7.68	4.52	7.30E-03
		47% overlap cross-section	0.5	7.01	4.67	7.50E-03
3	Four beads	30% overlap cross-section	0.42	13.8	4.45	7.50E-03
		47% overlap cross-section	0.52	10.66	4.26	7.10E-03

sultant quality. New layering tool paths need to be developed, but the tool path influences the results [1, 13, 26]. Here, this research will quantify a surface coating problem (2D) for a variable overlap percentage scenario to understand the influence of the percentage overlap on the mechanical properties.

2 Experimental design

To explore the influence of variable overlap on the bead geometry (width, height, and melt pool depth), distortion, and hardness, a 2400 W power level was utilized with a 4.4-mm laser spot size. This was kept constant throughout all the experiments. The torch angle was 90 degrees to the substrate. AISI 420 powder (55 ~ 160 μm grain size) was delivered through a co-axial nozzle onto a mild steel substrate (AISI 1018) through a concentric nozzle with argon gas, and the feed rate was 19 g/s. The chemical compositions of the materials are shown in Table 1. Argon gas was used as carrier for

Fig. 8 Bead cross-sections at the beginning (30% overlap) and end (47% overlap) for the 100-mm length sample

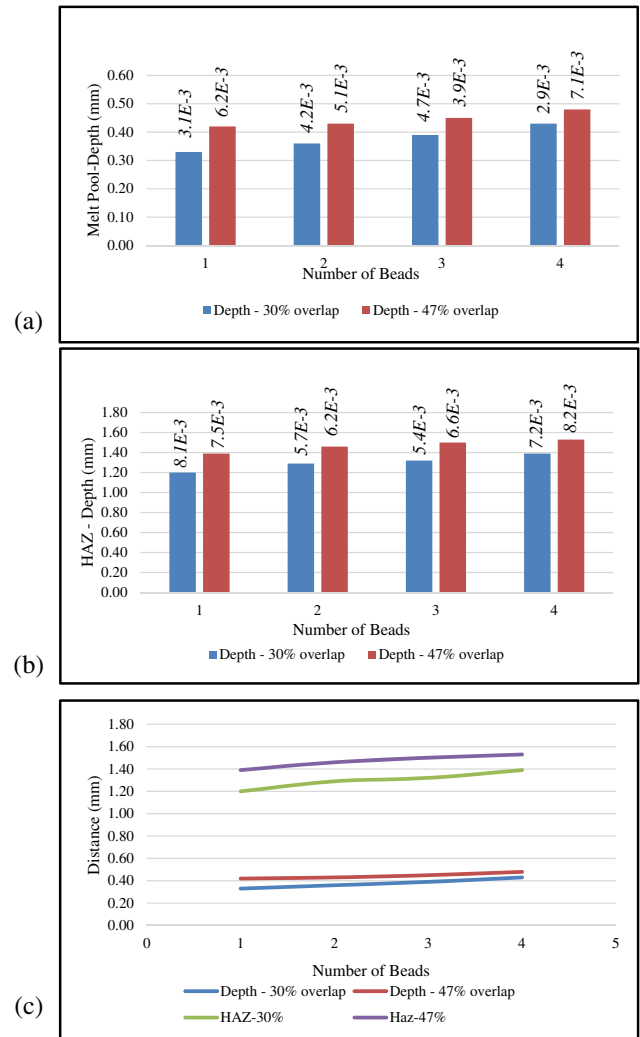
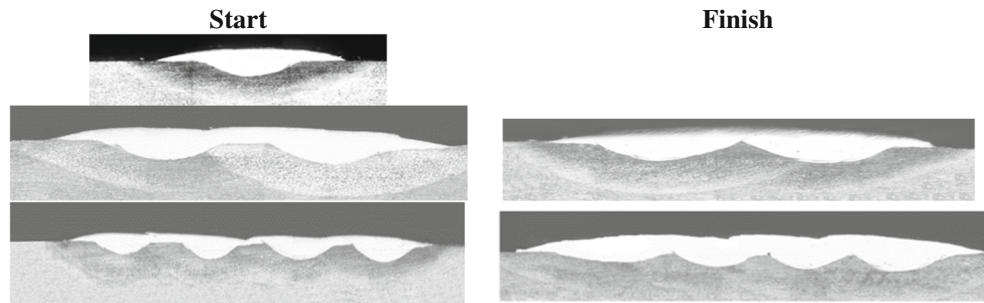
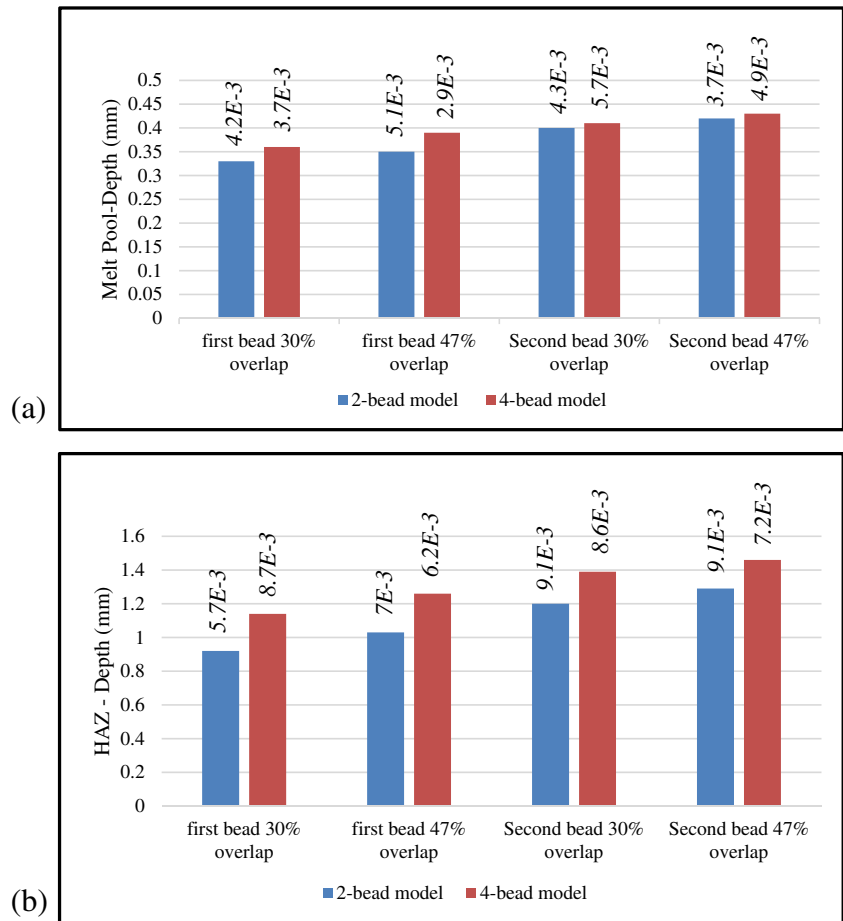


Fig. 9 a Melt pool depth or penetration with the standard deviations, b heat affected zone (HAZ) depth with the standard deviations, c a comparison of the trends (100-mm sample)

the powder and as a shielding gas in order to ensure powder conveyance and to limit oxidation. The nozzle assembly was a part of the laser beam delivery head and was mounted on the Z axis, while the workpiece stayed stationary. To avoid a potential time of lag between powder hopper and the melt pool, the powder feeder was turned on 5 s before the deposition starts.

Fig. 10 **a** Melt pool depth or penetration comparing two-bead data, **b** heat affected zone comparing two-bead data (100-mm sample)



The experimental procedures are summarized in a flowchart shown in Fig. 2.

In this study, the process parameters were constant values listed in Table 2. Six samples with three replicates were generated. Sets of substrate plates of various lengths were prepared with reference data collection features. The width and thickness were constant for all experiments. The designed overlaps at the beginning and end of the transition zones are 30% and 50%. There is a 10-mm lead in and lead out zone where the overlap percentages are constant throughout. Three samples have a 180-mm length, and the other three samples have a 100-mm length. There is a 10-mm distance from the plate edge to the beads; therefore, the bead lengths are 160 and 80 mm, respectively, and the variable overlap sections are 140 mm and 60 mm in length. For all the samples, a one-way deposition pattern was used. APlus® was used to generate the G codes for the tool paths once the bead lengths and regions of constant and variable overlap were established. The cladding strategy with the tool path directions is depicted in Fig. 3.

2.1 Distortion measurements

A Speed Grinder & Polisher with an Automet 3000 Power head was used to polish the base plates prior to deposition.

Distortion measurements were conducted on the face of the specimens which was not clad. In order to have the same reference level for distortion measurements, the basic 3-2-1 fixturing principle was used. Three 3-mm holes were drilled through the plates. The same three locations were used on each specimen. Ball bearings were placed underneath the holes on the surface plate. This established a planar surface for reference and a stable, static method for locating all samples, and distortion measurements were carried out using probe indicator (Fig. 4a), as it shows the direction of measurement is the Z axis. A reference grid is etched on the back face to provide data collection reference points (Fig. 4b).

The displacement in each point was measured for three different replicates, and the average of distortion for each point of the samples is used for the analysis.

The displacement measurements in each point on the specimens were measured before and after laser cladding. The distortions for the substrate plates were measured before the deposition of the clad beads to determine the initial substrate conditions. Figure 5 shows the displacement of all the samples before the deposition for both 100- and 180-mm lengths. As it can be seen, the displacements before cladding were negligible. The differences between the pre- and post-process measurements were

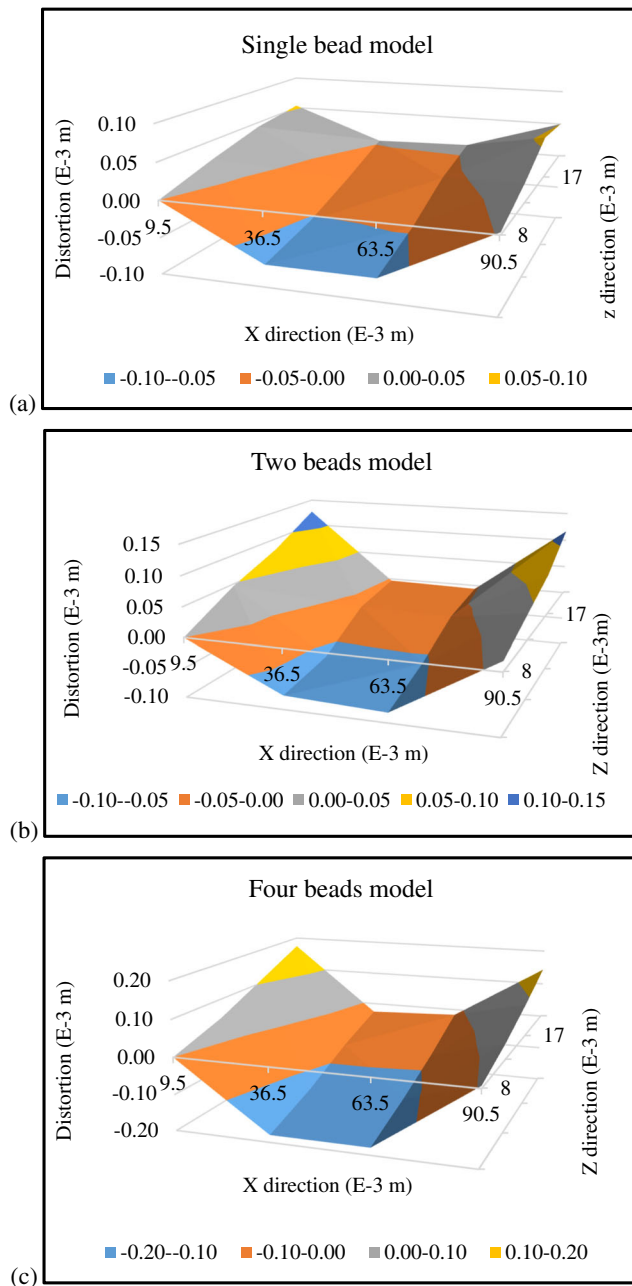


Fig. 11 Measured distortion for **a** a single bead, **b** two beads, and **c** three beads (100-mm samples)

used to calculate the final distortion of the plates, and the results were averaged for the three replicates.

2.2 Hardness measurement

In all samples, the hardness was measured in pairs with the Vickers hardness test equipment. A calibrated machine was used to apply 200 grams-force using a diamond indenter for 12 s. For the single-track models, the hardness measurement was conducted 10 mm from the beginning and the end of the clad beads. For the multi-track models, the hardness

measurement was carried out at the end of the 30% overlap section and at the beginning of the 50% overlap section (see Fig. 3). The hardness was measured within the bead, in the dilution zone, and in the substrate. Figure 6 shows the hardness measurements points.

3 Results

Laser-cladded samples of AISI 420 prepared by variable overlapping are displayed in Fig. 7. The effect of the change of the overlap is very evident for the four-bead samples, as the width is noticeably narrower. It was determined that 47% overlap occurred, although the programmed overlap was 50%. The enclosed regions are the constant overlap regions for the 47% (observed overlap) and 30% overlap.

3.1 Geometry measurements

The absolute geometry values are presented in Table 3, and a sample cross-section is illustrated in Fig. 8. The single bead is used as a reference size for finding the other sizes by the ImageJ software. Based on the percentage overlap, the approximated bead width is determined. It is challenging to measure the bead width, as some rotation occurred, which also influences the bead height. The maximum measured range was ± 0.05 mm. Therefore, the geometry generated by this process is repeatable.

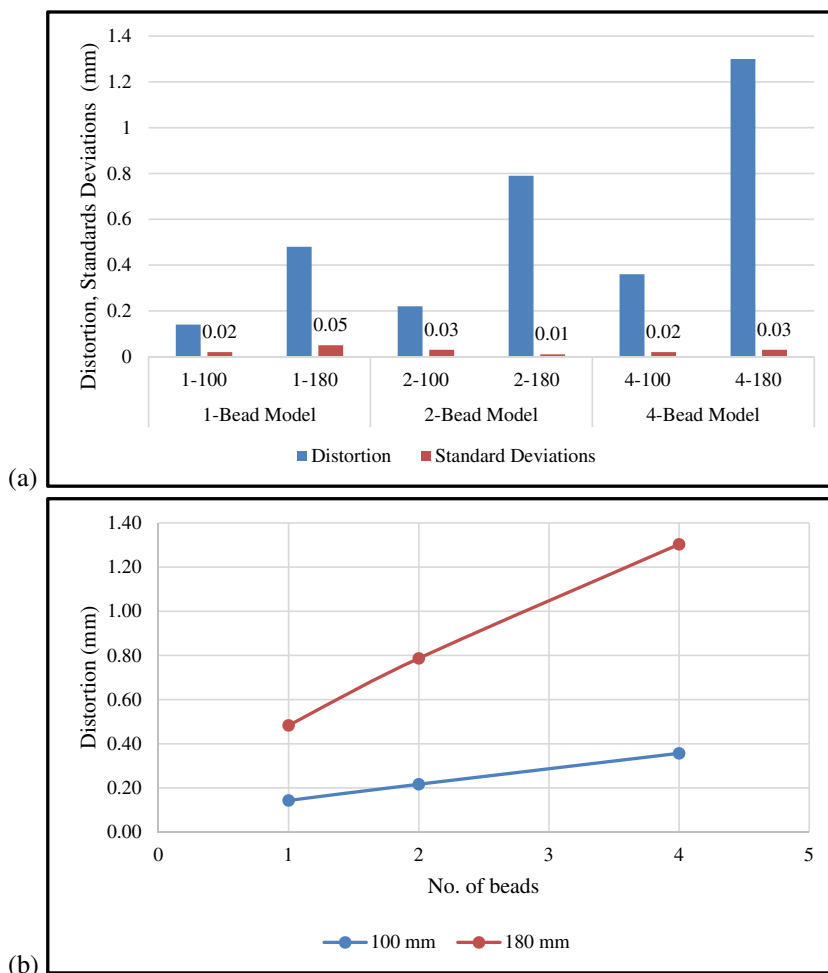
Previous experimental data was leveraged to define a tolerance interval with a 90% confidence level. This generated the following tolerance ranges when considering a wide band of operating conditions [27] for each shape parameter:

- Width: nominal predicted bead value ± 0.54 mm
- Height: nominal predicted height value ± 0.22 mm
- Penetration: nominal predicted value ± 0.22 mm

Here, the nominal value for the bead width is 4.41 mm, which correlates to the laser spot size, and the observed data falls within this tolerance range.

The bead height increases with the increasing overlap percentage. With a 30% overlap, the bead centre is not impacted, but with the higher percent overlap, the material can be placed onto the centre, and a slight increase is observed. This condition is challenging to denote for a representative simulation model. With a variable overlap percentage condition, not only does the height of the beads change along the deposition path (by approximately 25%), but the contact surface between each two adjacent beads is not constant. Based on these reasons, the representative geometric models are highly unstructured. A structured mesh cannot be readily generated without

Fig. 12 Measured distortion for **a** the absolute averaged values for the distortion data with the standard deviation values for the distortion experiments and **b** observed trends



manipulating surface geometry and strategically segmenting the geometry.

The influence of the bead overlaps on the melt pool and the heat affected zones (HAZs) is more significant. The influence of both the number of beads and the overlap is illustrated in Fig. 9 for the 4-bead test scenario for the 100-mm sample. The standard deviations for the data measured from the three replicates are shown in Fig. 9 in italics.

The depth and HAZ regions both increase, but interestingly, the differential between the them is relatively constant (Fig. 9c). The average distance between the depth and HAZ is 0.92 mm for the 30% overlap region and 1.03 mm for the 47% region. The standard deviation for both conditions is 0.04 mm.

When comparing the two-bead scenario to the first two beads of the 4-bead experiment, there is little difference in the observed data for the depth (Fig. 10a), and this differential (average = 0.02 mm) is well within the calculated predicted penetration variations. However, the HAZ variations are more significant and have a depth difference 0.25 mm on average (Fig. 10b). The standard deviations

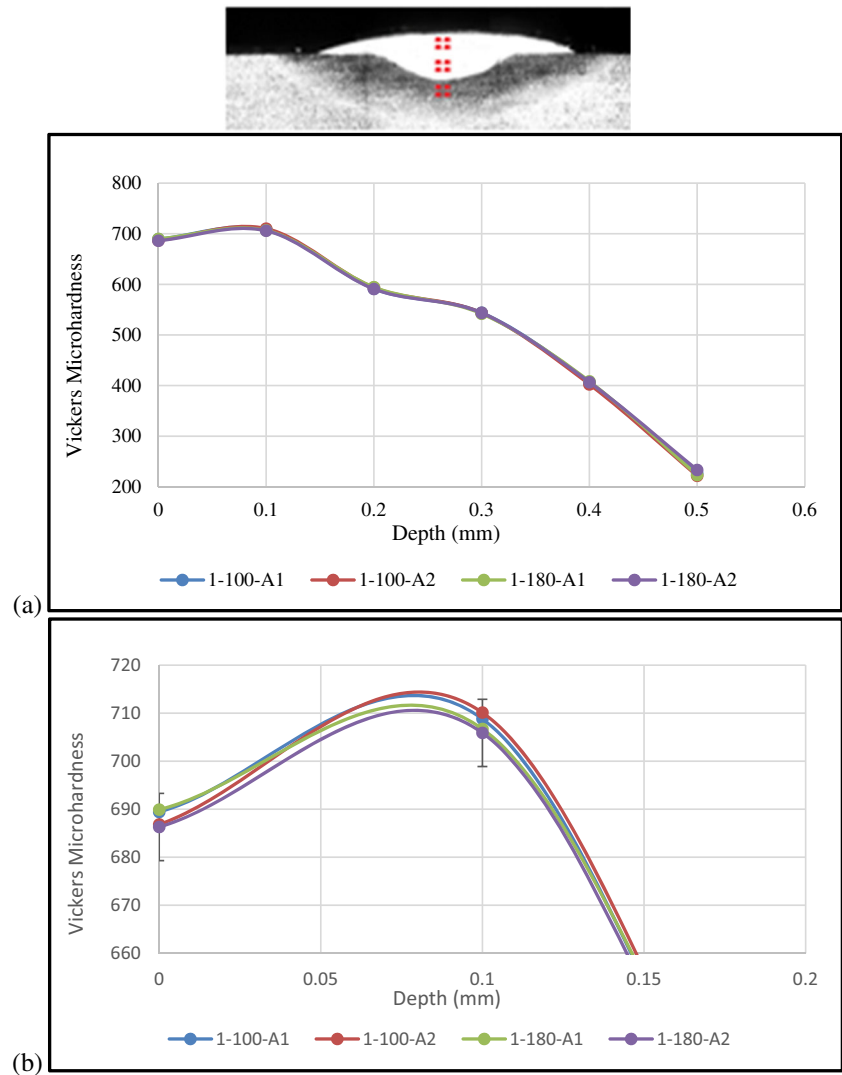
for the data measured from the three replicates are shown in Fig. 10 in italics.

When considering the depth along the length, the bead depth increases approximately 20% for the 100-mm sample, and for the 180-mm sample, the depth increased approximately 30%. When comparing the side-to-side conditions, the depth measurements are consistent for beads one and two for both the two-bead and four-bead samples for both the 100- and 180-mm scenarios.

3.2 Distortion results

The distortion measurements indicate that the number of beads and the length influence the observed distortion and that the observed repeatability shows that the distortion characteristics are very consistent. The observed standard deviations for each sample vary between 0.02 and 0.05 mm, and the average standard deviation is 0.02 mm. There is no difference in variability between the 100- and 180-mm specimens. The curved surfaces for a single track, a 2-bead set, and a 4-bead set for the 100-mm substrate samples are presented in Fig. 11.

Fig. 13 **a** A graphic illustrating the measurement strategy and the hardness profiles for all single-bead measurements, **b** hardness data for points 0- and 0.1-mm depth



A summary graph for the observed distortion with the standard deviations is shown in Fig. 12a. There is an offset ‘U’ shape, and the shape trends are consistent for all samples. The magnitude of the ‘U’ high and low points varies linearly, as shown in Fig. 12b.

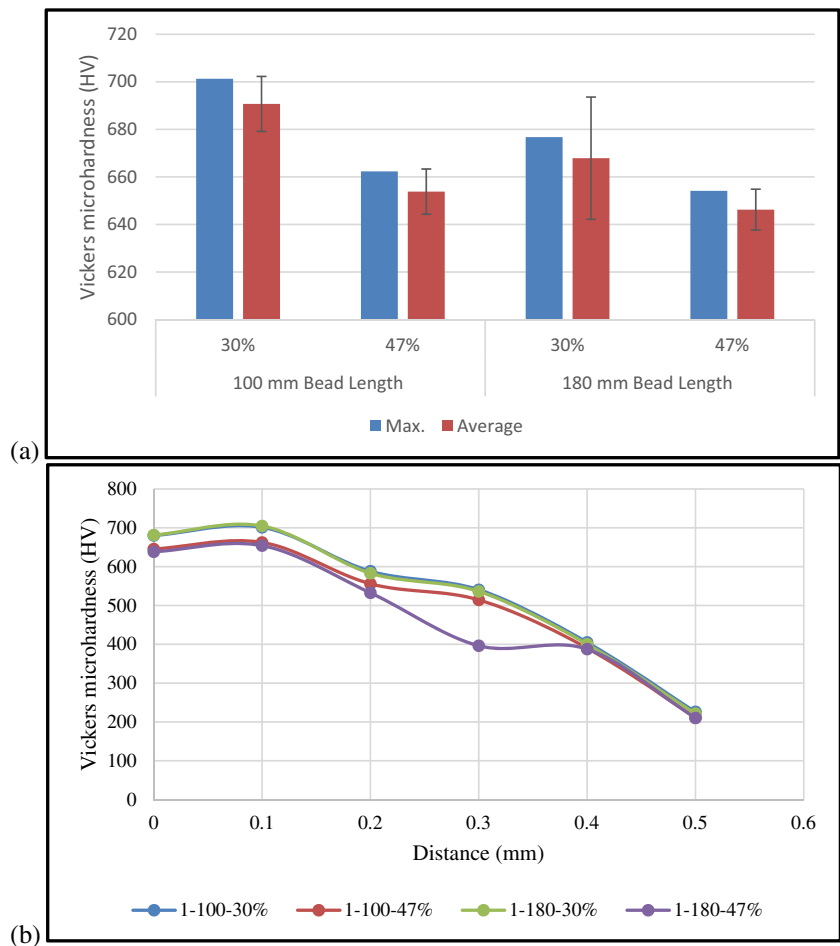
3.3 Hardness results

The hardness results for one bead were measured at $x = 10$ mm and $x = \text{bead length} - 10$ mm for the 100- and 180-mm length samples and are plotted in Fig. 13. Two sets of data are collected at the centre line of the first bead at various depths. There is essentially little variation in the observed results, as shown in Fig. 13b.

This information is a base line for subsequent analyses. The maximum hardness values occur at depth = 0.1 mm and are 708 HV, with a standard deviation < 2 HV. The average hardness is assessed using the data collected at points 0 and 0.1 and is 698 HV. The standard deviation is 11 HV.

The data for the two-bead configurations is plotted (Fig. 14) for the 100-mm and 180-mm scenarios (bead length is 80 mm and 160 mm, respectively). The hardness data is higher for the 100-mm specimens. There are shifts in the maximum and average values for each scenario, but the differential between the maximum and average is constant (8–10 HV). There is an approximately 3.4% reduction in maximum hardness for the 160-mm bead length experiment at the $x = 10$ mm measurement point when comparing to the 100-mm plate sample (677 HV as compared with 701 HV for the maximum). There is more heat added to the plate as the deposition time is 110.7 s for this sample set versus 5.3 s for the 80-mm length bead. The difference in hardness between the 80- and 160-mm samples for the 47% overlap is minimal and is consistently 8 HV. A shift in the hardness is observed at the 0.3-mm measurement depth. This phenomenon is observed for the hardness data for the 4-bead experiments (Fig. 15) for both the 100- and 180-mm sample lengths (Fig. 15b). A 140 HV

Fig. 14 **a** Hardness data summary for two-bead measurements with error bars indicating the standard deviations, **b** hardness curves showing the shifts between the 30 and 47% overlap data



hardness differential is observed for the 4-bead sample, which corresponds closely to the two-bead scenario results.

A comparison of the averaged hardness at the top of the bead for all experimental configurations is presented in Fig. 16. These results show that the travel length has essentially no effect on the hardness, the number of beads has a slight effect, and the percentage overlap has a significant effect. This research indicates that underfill areas will be harder for this material.

4 Discussion

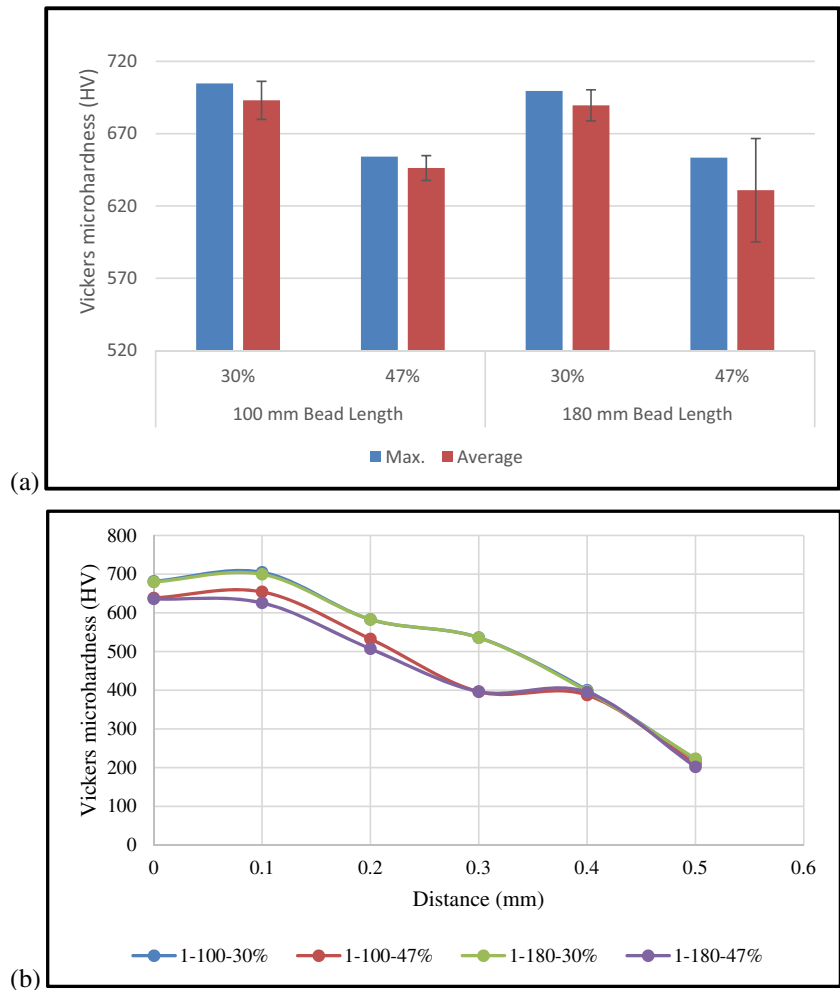
This study was carried out to find the effect of the percent overlap and the bead lengths (process time) on distortion and hardness and their sensitivity. The percentage overlap (30–47%) was chosen to replicate a reduced fill or partial fill scenario, as one would observe at a boundary-fill junction. As expected, increasing the overlap percentage changes the observed height, and the observed difference is approximately 25% greater for these conditions. This height change, and the angled bead placement, introduces meshing challenges for a

finite element model, but these variants are realistic issues to be addressed.

The melt pool depth increased from the first to the fourth bead. Additional investigations need to be performed to determine when the melt pool depth stabilizes. If a process designer provides a desired bead geometry (width, height, depth), it is reasonable to assume that variable process settings need to be introduced until a steady-state or quasi-steady-state point is reached. As the laser cladding process is highly coupled, changing the travel speed or other process setting will impact all geometry characteristics; this is not a trivial challenge. Varying the process settings as the material is being deposited will also impact the mechanical properties.

In the laser cladding process, the heat source moves across the plates with high energy. The substrate surface is heated and melted by a high power heat source. Simultaneously, the powder is fed into the melt pool to make a layer of coating. The large amount of heat causes the sample to have a very high temperature and a very sharp thermal gradient. After deposition, the high thermal gradient causes the plate to contract quickly which causes distortion. In the plates with the higher length, the heat input has been applied for a longer time

Fig. 15 **a** Hardness data summary for four-bead measurements with error bars indicating the standard deviations, **b** hardness curves showing the shifts between the 30 and 47% overlap data



which has caused larger distortion in the samples. However, the bead length change is double, but the observed increase in distortion varies from approximately 4 to 5 times more (Table 4). The number of deposited clad beads has direct relation with distortion, which is summarized in Table 5. It

is interesting to note that the 4-bead to 2-bead distortion ratio is almost constant for both length samples.

To consider the influence of the percentage overlap on distortion, the displacement data is compared for each sample (italicized data sets in Table 6). The displacement data patterns

Fig. 16 Average hardness data summary for all experimental configurations at the '0' distance

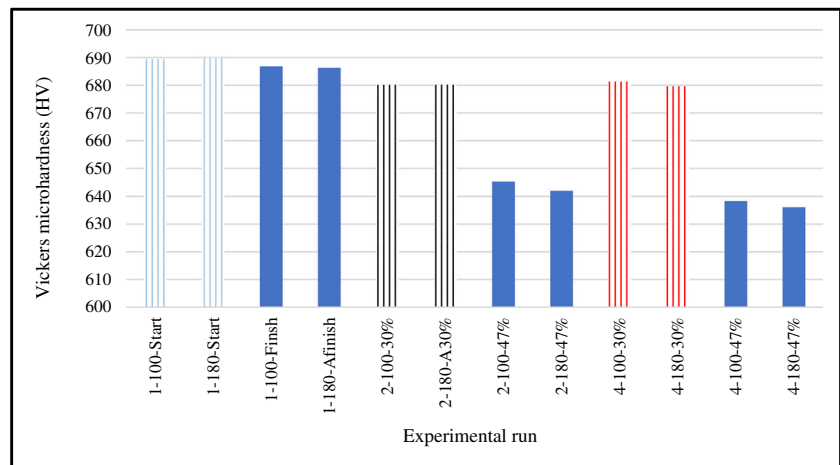


Table 4 Distortion ratio of 180-mm samples to 100-mm samples

	Single bead	Two beads	Four beads
Ratio	4.7	5.4	3.9

were very consistent for the initial and end measurement point sets for each data set. It can be concluded that the percent overlap has no influence on distortion, which is like the results reported by Ocelik et al. [20].

The distortion results are very repeatable. The maximum standard deviation for all distortion experiments is 0.05 mm. The deposition pattern was one way for this experiment; consequently, different results could be observed with a zigzag pattern as prior research indicated that the deposition pattern influences distortion and hardness. Consequently, simulations need to be conducted to explore these phenomena further.

In general, the hardness profile for the laser-cladded AISI 420 onto AISI 1018 is divided into two zones, namely, the cladding zone with high hardness values and the heat affected zone (HAZ) with lower hardness. The microhardness enhancement in the cladding zone is expected due to the chemical compound formation of AISI 420 and the rapid cooling rates associated with the laser cladding process. The measurements revealed that the variable overlapping causes the hardness not to be homogeneous along the clad beads. By comparing the surface and averaged hardness of the single-bead model with the averaged hardness of the first bead in 30% and 47% overlap cross-section of all samples, it is determined that the hardness is very sensitive to the amount of overlap. Hardness is affected by the cladding strategy as well as the thermal cooling rate which in turn depends on the conditions of the process. The areas at the beginning of overlap variation have higher hardness due to the martensitic microstructure formed due to the rapid cooling rate. As the deposition progressed, the overlap percentages increased, and the hardness reduced as a result of a slower cooling rate. The number of beads also influences the hardness, but the influence of the subsequent side-to-side bead deposition onto the substrate is dependent on the percentage overlap. Therefore, there are several contributing factors introducing hardness transients within the clad regions, which in turn impact the final product quality. New additive manufacturing tool paths are being developed. Spiral and raster morphing and square wave types of tool paths are being introduced. This research has shown the

Table 5 Distortion ratios for the number of beads

Ratio	2 beads/1 bead	4 beads/2 beads
100-mm length	1.51	1.65
180-mm length	1.63	1.66

Table 6 Measured displacement data (mm) for sample C1—180-mm sample

C1	10	50	90	130	170
8	0	0.53	0.7	0.50	0
12.5	- 0.19	0.35	0.54	0.35	- 0.16
17	- 0.40	0.17	0.36	0.17	- 0.36
21.5	- 0.57	- 0.02	0.18	0	- 0.52

importance of assessing the mechanical and physical characteristics of a tool path in addition to addressing the geometric requirements. In addition to voids, potential hardness variations need to be identified and managed.

The results of this study are summarized in Fig. 17.

5 Summary and conclusions

High power-based cladding is an economical process for repairing or building valued components and coating the substrates. Based on the complexity of the parts which are intended to be coated with a laser cladding process, using a constant overlap between adjacent clad beads either is not possible or may lead to voids or underfill regions. Variable overlap conditions commonly occur as a result of a standard raster fill tool path strategy. The component geometry and the tool path options influence the resultant voids and the build geometry, but challenges exist for convex hull geometry or components with several internal features (boundaries). To address void and underfill regions, a solution to reduce the uncoated spots on the substrate surface—controlled variable overlaps—is introduced and evaluated in this study. Eighteen samples were experimentally produced in 6 different conditions. Nine samples have 100-mm base plate length, and the rest of them have a 180-mm base plate length.

Overlap Percentage	Melt pool depth	↑
	Hardness	↓
	Distortion	→
Number of beads	Melt pool depth	↑
	Hardness	↓
	Distortion	↑
Sample length	Melt pool depth	→
	Hardness	→
	Distortion	↑

Fig. 17 Research trend summary

The measured bead geometry is consistent. The planned overlap percentages were 30% and 50% overlap, but 47% overlap was observed and recorded.

The overlap percentage influenced the melt pool depth and the hardness but had no influence on distortion. Therefore, the cases with round surface would not experience variable curling values at the edges where the percentage overlap changes, but the dilution and the hardness values will be different. In the multi-track models, the hardness in the cross-sections with the 30% overlap is higher than the hardness in cross-sections with a 47% overlap percentage. It is because of these regions having a higher cooling rate.

The number of beads influences all the measured factors, and continued research needs to be performed to determine whether the distortion trends continue to be linearly increasing. Research by Nazemi and Urbanic indicated that the surface area and aspect ratio (length/width) influence the observed distortion [12] but no linear trends were observed for those case studies. Consequently, significant insights could be extracted by exploring simulations for various substrate shapes and cladding conditions to determine if general trends could be extracted from these results.

The sample length has no influence on the hardness or melt pool depth, which eliminates some experimental factors.

This work will be extended to develop a calibrated numerical simulation model and will be used to provide insights for the intermediate regions for these experiments. This model will be extended to be used for multiple layers and thin wall bead stacking scenarios.

Funding information The support provided by MITACs, CAMufacturing Solutions, Inc., and Lincoln Laser Inc. are gratefully acknowledged.

References

- Wang C, Gao Y, Wang R, Wei D, Cai M, Yaokun F (2018) Microstructure of laser-clad Ni60 cladding layers added with different amounts of rare-earth oxides on 6063 Al alloys. *J Alloys Compd* 740:1099–1107
- Weng F, Chen C, Yu H (2014) Research status of laser cladding on titanium and its alloys: a review. *Mater Des* 58:412–425
- Adebiyi DI, Popoola API (2015) Mitigation of abrasive wear damage of Ti-6Al-4 V by laser surface alloying. *Mater Des* 74:67–75
- Tabernero I, Lamikiz A, Ukar E (2014) Modeling of the geometry built-up by coaxial laser material deposition process. *Int J Advanced Manuf Technology* 70:843–851
- Aggarwal K, Urbanic RJ, Saqib SM (2018) Development of predictive models for effective process parameter selection for single and overlapping laser clad bead geometry. *Rapid Prototyp J* 24: 214–228
- Ermurat M, Arslan MA, Erzincanli F, Uzman I (2013) Process parameters investigation of a laser-generated single clad for minimum size using design of experiments. *J Rapid Prototyp* 19: 452–462
- Nabhani M, Razavi RS, Barekat M (2018) An empirical-statistical model for laser cladding of Ti-6Al-4 V powder on Ti-6Al-4 V substrate. *Opt Laser Technol* 100:265–271
- Tran HS, Tchuindjang JT, Paydas H, Mertens A, Jardin RT, Duchêne L, Carrus R, Lecomte-Beckers J, Habraken AM (2017) 3D thermal finite element analysis of laser cladding processed Ti-6Al-4 V part with microstructural correlations. *Mater Des* 128:130–142
- Wang W, Wang M, Jie Z, Sun F, Huang D (2008) Research on the microstructure and wear resistance of titanium alloy structural members repaired by laser cladding. *Opt Laser Technol* 46:810–816
- Ochonogor OF, Meacock C, Abdulwahab M, Pityana S, Popoola API (2012) Effects of Ti and TiC ceramic powder on laser-cladded Ti-6Al-4 V in situ intermetallic composite. *Appl Surf Sci* 263:591–596
- Weng F, Yu H, Chen C, Liu J, Zhao L, Dai J, Zhao Z (2017) Effect of process parameters on the microstructure evolution and wear property of the laser cladding coatings on Ti-6Al-4 V alloy. *J Alloys Compd* 692:989–996
- Nazemi N, Urbanic RJ (2018) A numerical investigation for alternative toolpath deposition solutions for surface cladding of stainless steel P420 powder on AISI 1018 steel substrate. *Int J Adv Manuf Technol* 96:9–12
- Paydas H, Mertens A, Carrus R, Lecomte-Beckers J, Tchuindjang JT (2015) Laser cladding as repair technology for Ti-6Al-4 V alloy: influence of building strategy on microstructure and hardness. *Mater Des* 85:497–510
- Farayibi PK, Abioye TE, Clare AT (2016) A parametric study on laser cladding of Ti-6Al-4 V wire and WC/W2C powder. *Int J Adv Manuf Technol* 87:3349–3358
- Nazemi N, Alam MK, Urbanic RJ, Saqib S, Edrissy A. “A hardness study on laser cladded surfaces for a selected bead overlap conditions.” Springer. SAE Technical Paper. 2017-01-0285
- Lindgren L-E (2001) Finite element modeling and simulation of welding part 1: increased complexity. *J Therm Stresses* 24:141–192
- Chiumenti M, Cervera M, Salmi A, de Saracibar CA, Dialami N, Matsui K (2010) Finite element modeling of multi-pass welding and shaped metal deposition processes. *Comput Methods Appl Mech Eng* 199:2343–2359
- Fessler J, Merz R, Nickel A, Prinz FB, Weiss L (1996) Laser deposition of metals for shape deposition manufacturing. *Proc Solid Freeform Fab Symp*:117–124
- Klingbeil NW, Beuth JL, Chin RK, Amon CH (2002) Residual stress-induced warping in direct metal solid free form fabrication. *Int J Mech Sci* 44:57–77
- Vayre B, Vignat F, Villeneuve F (2013) Identification on some design key parameters for additive manufacturing: application on electron beam melting. *Procedia CIRP* 7:264–269
- Grum J, Žnidaršič M (2004) Microstructure, microhardness, and residual stress analysis of laser surface cladding of low-carbon steel. *Mater Manuf Process* 19:243–258
- Plati A, Tan J, Golosnoy I, Persoons R, Van Acker K, Clyne T (2006) Residual stress generation during laser cladding of steel with a particulate metal matrix composite. *Adv Eng Mater* 8:619–624
- Ocelík V, Bosgra J, de Hosson J (2009) In-situ strain observation in high power laser cladding. *Surf Coat Technol* 203:3189–3196
- Zinovieva O, Zinoviev A, Ploshikhin V (2018) Three-dimensional modeling of the microstructure evolution during metal additive manufacturing. *Comput Mater Sci* 141:207–220

25. Liu H, Hao J, ZhengtongHan GY, XiuliHe HY (2016) Microstructural evolution and bonding characteristic in multi-layer laser cladding of NiCoCr alloy on compacted graphite cast. *J Mater Process Technol* 232:153–164
26. Nazemi N, Urbanic RJ (2017) An experimental and simulation study for powder injection multitrack laser cladding of P420 stainless steel on AISI 1018 steel for selected mechanical properties. *J Manuf Sci Eng.* 140
27. Urbanic RJ, Saqib SM (2019) A manufacturing cost analysis framework to evaluate machining and fused filament fabrication additive manufacturing approaches. *Int J Adv Manuf Technol* 102:9–12

Publisher's note Springer Nature remains neutral with regard to jurisdictional claims in published maps and institutional affiliations.